Electronic Supplementary Material (ESI) for Physical Chemistry Chemical Physics

Redox control of ferrocene-based complexes with systematically extended π-conjugated connectors: switchable and tailorable second order nonlinear optics

Wen-Yong Wang, Na-Na Ma, Shi-Ling Sun, and Yong-Qing Qiu*

Institute of Functional Material Chemistry, Faculty of Chemistry, Northeast Normal University, Changchun 130024, Jilin, People's Republic of China

* Corresponding Author. Fax: +86 431 85098768.
E-mail addresses: qiuyq466@nenu.edu.cn(Y. Q. Qiu)

Table S1. Calculated bond length alternation (BLA, Å) of 4,4'-bipyridinium moieties of the studied complexes.

complex	$[1]^{4+}_{open}$	$[2]^{4+}_{open}$	$[3]^{4+}_{open}$	$[4]^{4+}_{open}$
BLA	0.0535	0.0545	0.0462	0.0507
complex	$[1]^{2+}_{dim}$	$[2]^{2+}_{dim}$	$[3]^{2+}_{dim}$	$[4]^{2+}_{dim}$
BLA	0.0413	0.0423	0.0411	0.0409

Table S2. The β_x, β_y, β_z, and β_{tot} (10^{-30} esu) at various levels of theory.

	functional	β_x	β_y	β_z	β_{tot}
$[1]^{2+}_{dim}$	B3LYP	38.6	0.2	-0.4	38.6
	PBE1PBE	33.8	0.1	-0.3	33.7
	BHandHLYP	28.8	0.1	-0.3	28.8
	CAM-B3LYP	26.1	0.1	-0.3	26.1
	LC-BLYP	19.0	0.1	-0.2	19.0
	ωB97XD	23.3	0.1	-0.2	23.3
$[2]^{2+}_{dim}$	B3LYP	58.0	3.8	2.7	58.1
	PBE1PBE	33.4	22.2	2.0	33.5
	BHandHLYP	7.8	0.4	1.3	8.0
	CAM-B3LYP	8.9	0.4	1.4	9.0
	LC-BLYP	1.4	-2.0	1.5	2.9
	ωB97XD	6.4	0.1	1.4	6.6
$[3]^{2+}_{dim}$	B3LYP	60.6	-0.5	-1.1	60.6
	PBE1PBE	54.3	-0.5	0.9	54.3
	BHandHLYP	44.5	-0.3	5.7	44.9
	CAM-B3LYP	45.2	-0.4	5.4	45.6
	LC-BLYP	32.3	-0.2	13.4	35.0
	ωB97XD	40.4	-0.3	7.5	41.1
$[4]^{2+}_{dim}$	B3LYP	246.0	7.1	3.0	246.1
	PBE1PBE	199.9	5.7	2.4	199.9
	BHandHLYP	120.2	3.5	1.5	120.3
	CAM-B3LYP	97.3	2.8	1.2	97.4
	LC-BLYP	45.7	1.3	0.6	45.7
	ωB97XD	75.2	3.0	1.3	75.2

Electronic Supplementary Material (ESI) for Physical Chemistry Chemical Physics

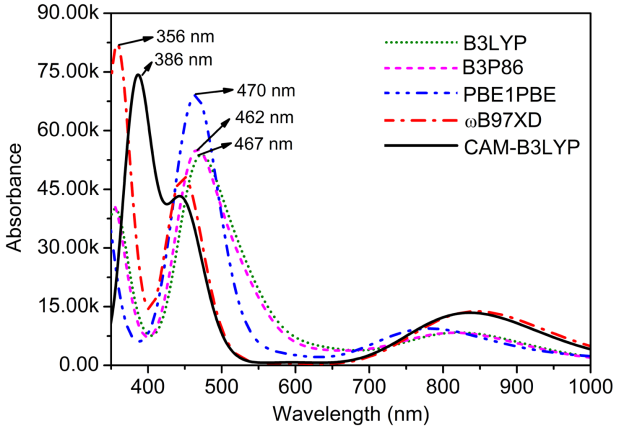

Fig. S1 Simulated absorption spectrum of complex $[4]^{2+}_{\mathrm{dim}}$ at various levels of theory.

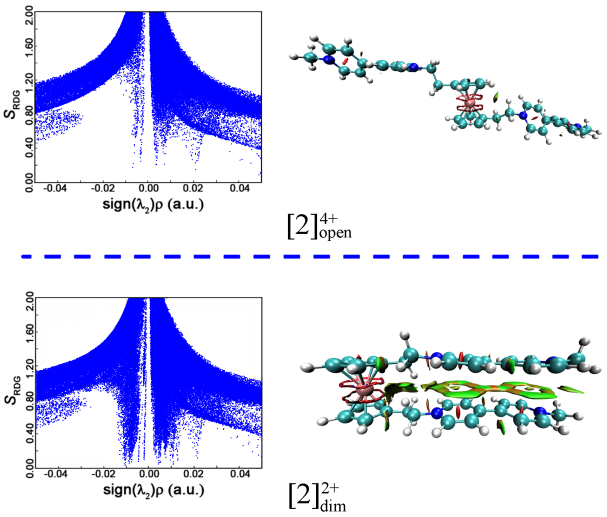

Fig. S2 Plots of S_{RDG} versus $\mathrm{sign}(\lambda_2)\rho$ and the gradient isosurface for $[2]^{4+}_{\mathrm{open}}$ and $[2]^{2+}_{\mathrm{dim}}$.

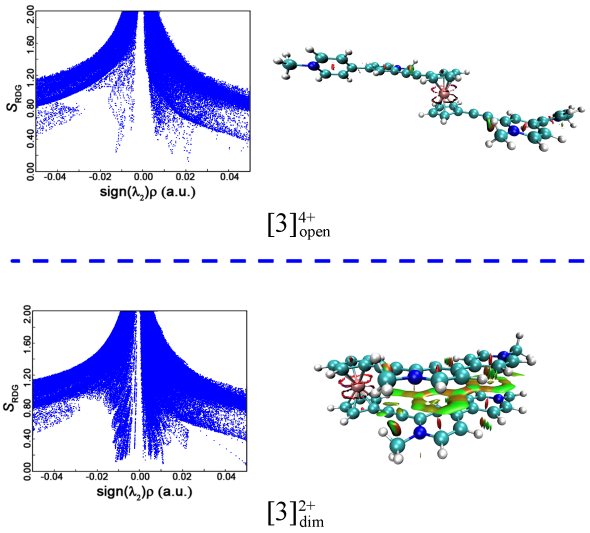

Fig. S3 Plots of S_{RDG} versus $\mathrm{sign}(\lambda_2)\rho$ and the gradient isosurface for $[3]^{4+}_{open}$ and $[3]^{2+}_{dim}$.

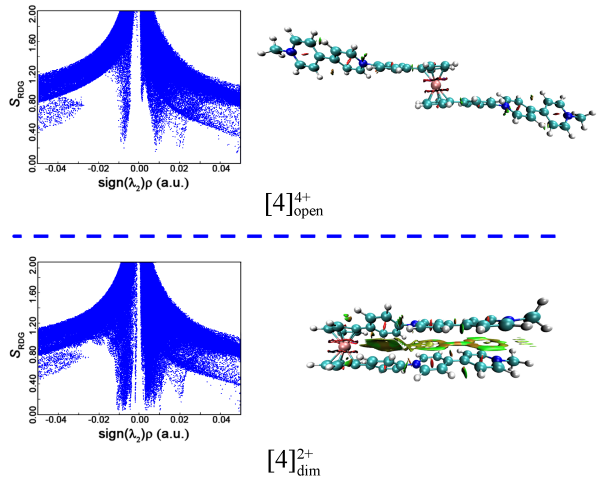

Fig. S4 Plots of S_{RDG} versus $\mathrm{sign}(\lambda_2)\rho$ and the gradient isosurface for $[4]^{4+}_{open}$ and $[4]^{2+}_{dim}$.

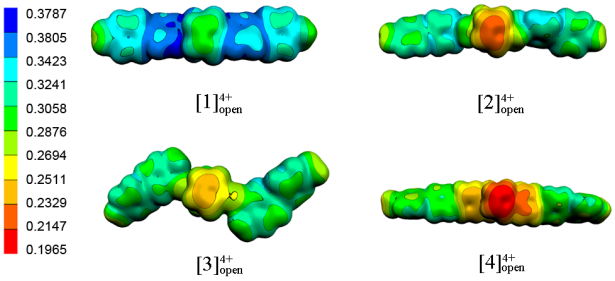

Fig. S5 Molecular electrostatic potential maps of complexes $[1]^{4+}_{open}$ -$[4]^{4+}_{open}$.

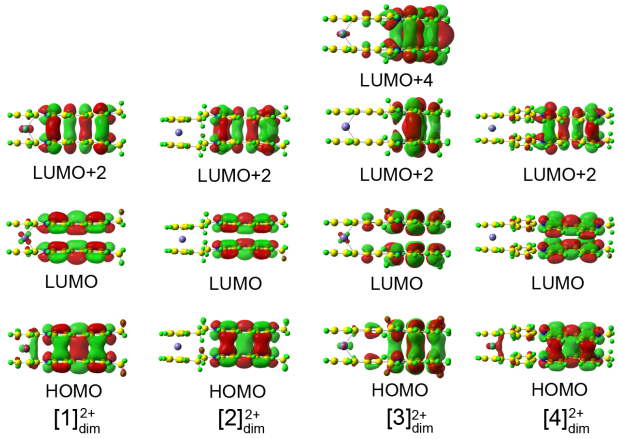

Fig. S6 The frontier molecular orbitals involved in the low-energy region and middle-energy region.

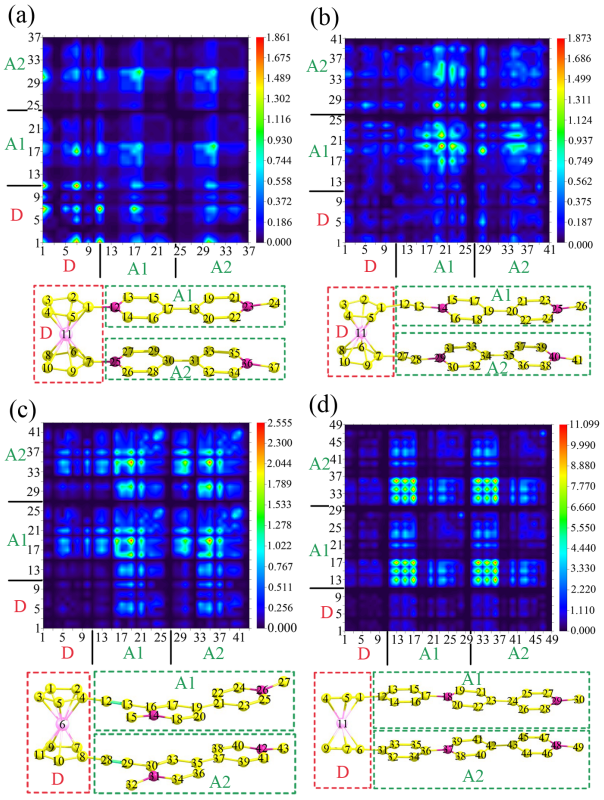

Fig. S7 The TDM corresponding to the middle-energy electronic transitions of complexes (a) $[1]^{2+}_{dim}$, (b) $[2]^{2+}_{dim}$, (c) $[3]^{2+}_{dim}$, and (d) $[4]^{2+}_{dim}$ (the hydrogen atoms have been omitted).

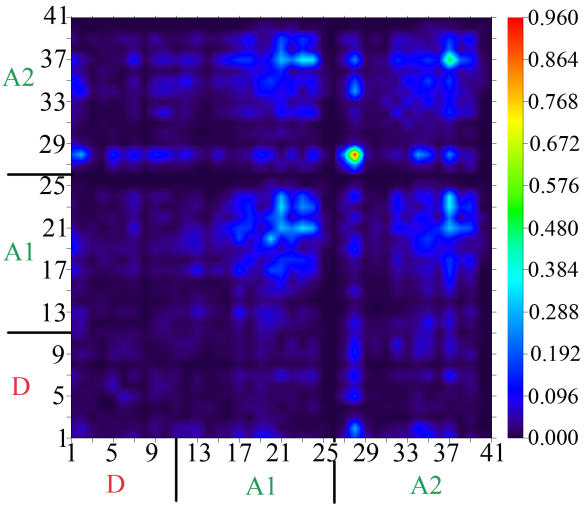

Fig. S8 The TDM associated with the S_{21} state of complex $[2]^{2+}_{dim}$ (absorbing at 292.9 nm) (the hydrogen atoms have been omitted).

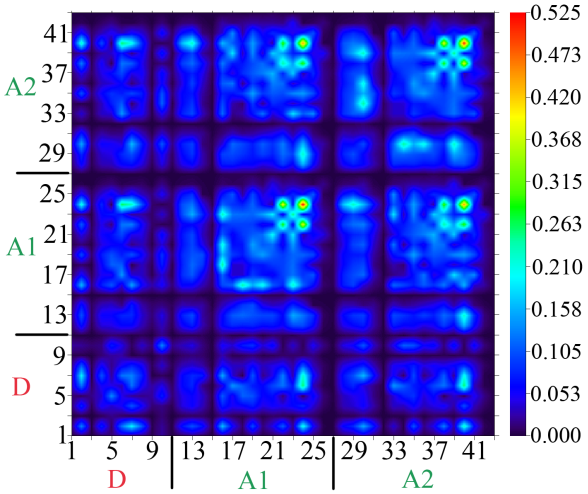

Fig. S9 The TDM associated with the S_{22} state of complex $[3]^{2+}_{dim}$ (absorbing at 293.7 nm) (the hydrogen atoms have been omitted).